Chapter 9

Radioactivity surveys

9.1 Introduction

Since the discovery of radioactivity (H. Becquerel, 1896), studies of the radioactivity of rocks and minerals have found applications in many fields of geology and geophysics. First, the rate of radioactive decay of certain naturally occurring elements in rocks provides a powerful means of dating geological events, in particular the times of formation of rocks. Second, the heat produced by radioactive disintegrations in various types of crustal rocks is of importance in studies of thermal conditions in the subsurface. Third, radioactivity surveys are of use in geological mapping as different rock types can be recognized from their distinctive radioactive signatures. Probably, the most common application of radiometric techniques is in geophysical borehole logging for estimation of rock porosity and detection of fractures and underground movement of fluids (Section 11.3.3).

Radioactivity is part of our physical environment. The largest contribution to the radiation field is of natural origin; it is due to cosmic rays, the natural radioactivity of the grounds, and the radioactive decay products of radon in the air. Artificial radioactivity is emitted by nuclear power plants, industrial plants, and some research laboratories. These emissions are very small in normal operation, although large amounts of radioactivity can be released to the environment through accidents. One of the most publicized was the nuclear accident at Chernobyl, Ukraine (April 26, 1986), which caused a serious concern because of the risk to public health in the areas affected by high levels of radiation exposure.

This chapter aims to provide a brief discussion of the principles and practices of radiometric survey methods. A few examples of applications to environmental problems such as localization of buildings with high indoor radon concentrations, radon monitoring of active faults and earthquake prediction, and detection of radioactive pollution in soil, groundwater, and air are included.

9.2 Fundamentals of radioactive disintegration

By the phenomenon of radioactivity we mean the disintegration of an atomic nucleus by emission of energy and particles of mass. The disintegrating nucleus ${}^{A}X_{Z}$ is transformed into a nucleus of another element with a change in atomic mass A and atomic number Z, the by-products of disintegration being **α particles** (helium nuclei, ${}^{4}He_{2}$), **β particles** (electrons), and **γ-radiation** in various combinations.

Radioactive disintegration or decay is a random process and is expressed in terms of the probability that a constituent particle in a nucleus will escape through the potential barrier binding it to the nucleus. The probability of decay is unaffected by physical conditions, like pressure and temperature, and depends upon the number of atoms present. It follows that the rate of decay of N nuclei of a particular species is directly proportional to N:

$$\frac{dN}{dt} = -\lambda N \tag{9.1}$$

of which the solution is

$$N = N_0 e^{-\lambda t} \tag{9.2}$$

where N_0 is the number present at time $t=0$. The factor λ, called the **decay constant**, is a unique property of each disintegrating nucleus.

The rate of decay is often quoted in terms of a related quantity, the **half-life**, $T_{1/2}$. This is the time (in seconds) taken to reduce the number of parent atoms by one-half. Therefore, putting $N=N_0/2$ and $t=T_{1/2}$ into Eq.(9.2) gives

$$\ln 2 = \lambda T_{1/2} \tag{9.3}$$

so that

$$T_{1/2} = 0.693/\lambda \tag{9.4}$$

Let us suppose that the decay of a radioactive parent produces a stable radiogenic daughter and that the number of daughter atoms is zero at $t=0$. The number of daughter atoms, D, produced by the decay of the parent N at any time is given by

$$D = N_0 - N \tag{9.5}$$

Substituting the expression for N_0 from Eq.(9.2) in Eq.(9.5), gives

$$D = N(e^{\lambda t} - 1) \tag{9.6}$$

Decay mechanisms and experimentally determined decay constants (λ) of important radioactive elements are listed in Steiger and Jaeger (1977). If λ is known, measurements of the relative abundance of a parent isotope and the end or daughter product permit the determination of t from Eq.(9.6). This is the basis of the radiometric dating methods.

Table 9.1 *Radiation measurement units and conversion factors.*

Unit	Definition	Conversion
R (roentgen)	Radiation required to produce 1 electrostatic unit (e.s.u.) of charge	1 e.s.u. charge $=2.083\times10^{15}$ ions/m^3
Bq (becquerel)	1 disintegration/s	1 Bq=27 pCi
Ci (curie)	Activity of 1 g of Ra	1Ci=3.7×10^{10} Bq
pCi/l	Activity measured in fluids	1 pCi/l=37 Bq/m^3
Gy (gray)	Absorbed dose corresponding to 1 joule (J) of radiation per kg of body tissue	1 Gy=100 rad
Sv (sievert)	Equivalent dose representing damage to tissue	1 Sv=1 J/kg
WL (working level)	Potential α-radiation concentration in air at a working place	1 WL=3740 Bq/m^3 (or 3.7 Bq/l)
WLM (working level month)	Exposure at a working place in 1 month (173 hours)	1 WLM=1 WL×173

The disintegration of a nucleus is accompanied by the emission of three possible types of energy or particles. α particles are helium nuclei ($^4He_2$) with two protons (positive charge, +2) and two neutrons. They are easily absorbed or stopped by a few sheet of paper. β particles are electrons which may be emitted when a neutron splits into a proton and an electron during certain disintegrations. β particles are stopped by a few milimeters of aluminium. γ-photons (commonly called γ-rays) are electromagnetic radiation released from excited nuclei during disintegrations. They are similar to X-rays but have shorter wavelength and higher energy content. Their penetrating capacity is much greater than that of α or β particles. Since α and β particles are readily stopped, even by the thinnest cover of overburden, it is mostly through the detection of γ-radiation that lithologies can be mapped to help locate zones of anomalous radioactivity. Only γ-radiation can be detected in airborne surveys.

9.3 Units of radiation and dosage

A wide variety of units are used to measure radioactivity. Their definitions and conversion factors are given in Table 9.1. The standard unit for measuring γ-radiation (similar in nature to X-rays) is the roentgen (R). In geophysical work, a smaller unit, the microroentgen (1 μR=10^{-6} R) is commonly used.

Radioactivity can also be measured in terms of the rate of disintegrations; the units used are the becquerel (Bq) and the curie (Ci). In radon measurements, a

Table 9.2 *Radioactive decay series of uranium (^{238}U). Isotopes containing less than 0.25% of the decay products are omitted.*

Element	Z	Emission	Half-life
Uranium-238	92	α	4.51×10^{9} y
Thorium-234	90	β,γ	24.1 d
Protactinium-234	91	β,γ	1.18 min
		or β	6.7 h
Uranium-234	92	α	2.48×10^{5} y
Thorium-230	90	α	8×10^{4} y
Radium-226	88	α,γ	1622 y
Radon-222	86	α	3.825 d
Polonium-218	84	α,β	3.05 min
Lead-214	82	β,γ	26.8 min
Astatine-218	85	α	2 s
Bismuth-214	83	β,α,γ	19.7 min
Polonium-214	84	α	1.6×10^{-4} s
Thallium-210	81	β,γ	1.3 min
Lead-210	83	β,γ	20 y
Bismuth-210	83	β,α	5.0 d
Polonium-210	84	α	138.4 d
Thallium-206	81	β	4.2 min
Lead-206	82	Stable	

smaller unit, picocuries per liter (pCi/l), is most commonly used in the U.S. and Canadian literature. The U.S. Environmental Protection Agency (EPA) recommends remedial action in indoor areas where radon levels are 4 pCi/l or above. The EPA potable water standard is 500 pCi/l; water with radon concentration above this level is not suitable for human consumption unless it is treated first.

The radiation dose absorbed by the body tissue is of prime interest in health physics. The absorbed dose defines the energy that is transferred to the body and is measured by the unit gray, rad, or sievert. Since the emission of alpha particles (by radon and other nuclides) can have harmful health effects, the working level (WL) is used to define the total alpha energy to which the body is exposed. The Swedish government regards an existing building as unsanitory at a level of 0.108 WL. For new buildings they have proposed a maximum limit of 0.0189 WL (=70 Bq/m^3).

9.4 Radioactive decay series and equilibrium

When a parent isotope disintegrates, very often the initial daughter product is also radioactive, and it decays, perhaps through a series of radioactive nuclei, until the stable end product is reached. Table 9.2 shows the ^{238}U decay series and includes the principal emissions and half-lives of the decay products.

Basically, a daughter product is in equilibrium with its parent when the numbers of daughter atoms, N_2, disintegrating per second is the same as the number being created by disintegrations of the parent atoms, N_1. When the entire decay series is in equilibrium, it follows from Eqs.(9.2) and (9.6) that

$$N_1\lambda_1 = N_2\lambda_2 = N_3\lambda_3 = \ldots N_n\lambda_n \tag{9.7}$$

For example, let us examine the state of radioactive equilibrium between the parent ^{226}Ra and the daughter ^{222}Rn in the decay series of Table 9.2. Here the daughter (half-life, $T_{1/2}$=3.825 days) decays about 155,000 times faster than its parent ($T_{1/2}$=1622 years). By using the equilibrium condition, that is, $N_1/N_2=\lambda_2/\lambda_1$, the equilibrium time, t_{eq}, can be related to the decay constants of the parent (λ_1) and the daughter product (λ_2). The relationship to achieve full equilibrium is given by

$$t_{eq} = \left(\frac{1}{\lambda_1 - \lambda_2}\right) \ln \frac{\lambda_1}{\lambda_2} \tag{9.8}$$

Using the decay constant values for ^{226}Ra ($\lambda = 1.35\times10^{-11}$/s) and for ^{222}Rn ($\lambda = 2.09\times10^{-6}$/s) the value of t_{eq} is about 66 days. In actual fact, full equilibrium (100%) is only approached asymptotically. The times required for ^{222}Rn to achieve effective equilibrium with ^{226}Ra at the 99% and 95% levels are, respectively, about 25 and 17 days.

In the case of a radioactive series with n products, the time required for establishing equilibrium is determined by the half-life of the isotope of longest life. Under equilibrium conditions it is possible to determine the amount of a parent product in a sample by measuring the amount of one of the succeeding members. If the series is not in equilibrium, for example because some member or members are reduced or missing due to preferential leaching or weathering, or leakage of radon gas, the count would be reduced and would cause a corresponding error in the calculation of the parent element.

9.5 Radioactivity of rocks

Measurements of the radioactive properties of naturally occurring substances indicate that a low level of activity is present in almost all rocks and minerals. Initially, this activity was attributed almost entirely to traces of uranium and thorium and their radioactive decay products. Later investigations showed that an isotope of potassium (^{40}K) is also radioactive. Although this isotope forms only 0.012% of the potassium in the earth's crust, it contributes very significantly to the radioactivity of rocks, because of the very widespread occurrence of potassium itself in the crustal rocks.

Table 9.3 gives an idea of typical abundances of uranium, thorium, and potassium in common rock types. Note that granites and shales have a relatively large content of uranium and thorium which makes them exhibit higher radioactivity

Table 9.3 *Typical abundances of important radioactive elements in various rock types.*

Rock type	U (ppm)	Th (ppm)	K (%)
Granite	5	18	3.8
Basalt	0.6	3	0.8
Shales	5	12	2.7
Sandstones	1	2	0.6
Limestones	1.8	1.6	0.3
Beach sands	3	6	0.3

than other rock types. Uranium and thorium frequently occur together in some rock minerals and their isotopes (^{238}U, ^{235}U, and ^{232}Th) decay eventually to stable isotopes of lead via intermediate daughter isotopes. Uranium and thorium isotopes have half-lives comparable to the age of the earth and hence they are still sufficiently abundant. In naturally occurring uranium, the ^{238}U isotope is the most abundant (99.28%).

Of principal interest in environmental radioactivity are the rock types that are enriched in uranium and thorium, and that serve as a source of radon (^{222}Rn) contamination in air, soil and groundwater. The most common sources are granite, black shale, pegmatites, phosphatic limestones and their metamorphosed equivalents.

9.6 Instruments for measuring radioactivity

9.6.1 Geiger counter and scintillometer

Of the many types of radiation detectors designed for field use, the **Geiger counter** is the simplest and cheapest. It consists of a sealed glass tube with a cylindrical cathode around a thin central wire anode. The tube is filled with an inert gas (usually argon with a trace of alcohol) and a high voltage is applied between the electrodes. Normally the gas is non-conducting, but when radiation enters the tube, the gas is ionized and the ions and electrons produced accelerate toward the electrodes. The resulting current pulses can be amplified and are registered on a meter or are heard as a 'click' in a pair of headphones. Since γ-rays are very weakly ionizing and α particles have such short ranges that they need not be considered generally, the instrument primarily responds to β particles.

The **scintillation meter** is a more efficient type of detector, in particular for γ-rays. It utilizes the fact that certain crystals such as thallium-activated sodium iodide emit a visible flash of light (scintillate) when they absorb γ-rays. The scintillations can be detected by photomultiplier tubes, and after suitable amplification can

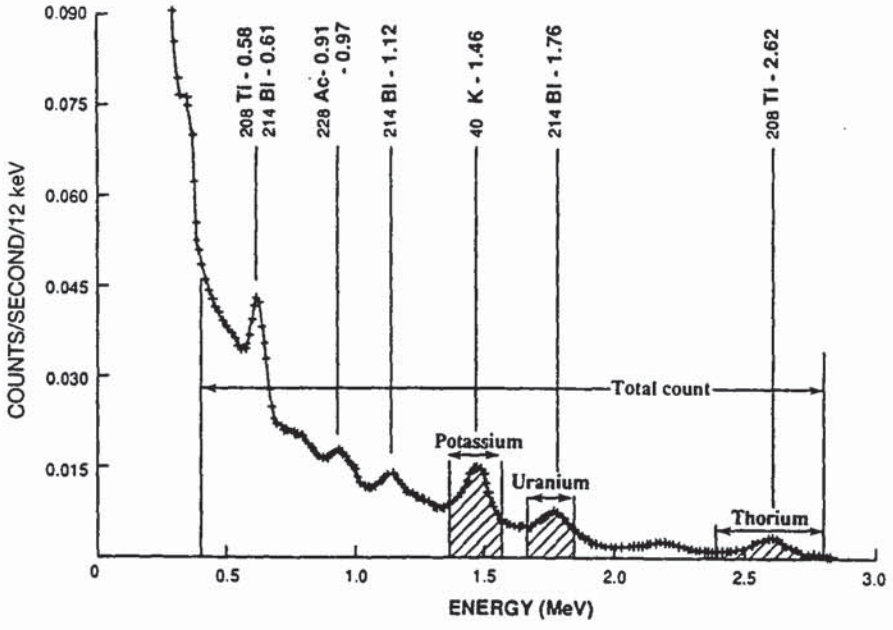

Fig. 9.1 A typical airborne gamma-ray spectrum showing the customary four windows: total count, 0.4–2.81 MeV; ^{40}K, 1.37–1.57 MeV; ^{238}U, 1.66–1.86 MeV; and ^{232}Th, 2.42–2.81 MeV. (After Grasty, 1987.)

be read on a meter in counts per minute. Because of its much greater efficiency (almost 100% for detecting γ-radiation), the scintillation meter has in many cases replaced the Geiger counter in modern work. Scintillometers are available which can be mounted in ground transport or aircraft and interfaced with strip recorders to yield plots of count rates. Obviously, scintillometers of the highest sensitivity are required in airborne work and flight heights must be kept relatively low ($\lesssim$50 m).

9.6.2 Gamma-ray spectrometer

The γ-ray spectrometer is an extension of the scintillometer that separates characteristics of γ-rays of potassium, thorium, and uranium isotopes for identification of the source. The instrument sorts the electrical pulses from the photomultiplier according to their energy into three or more ranges before recording the rate of arrival of pulses of each of the selected energy ranges. When potassium, uranium, and thorium are all present, the composite spectrum might look like the display in Fig. 9.1, in which the individual lines have been broadened by the low-resolution thallium-activated sodium iodide crystal used in the detection instrument.

Assuming equilibrium, the concentrations of the parent nuclides can be determined by measurement of the γ-radiation produced by the daughter. In standard practice, four quantities are measured in γ-ray spectrometry: (1) TC=total count integrated under the spectrum between 0.4 and 2.81 MeV; (2) ^{40}K=potassium

content via integrated count between 1.37 and 1.57 MeV (the so-called 1.46 MeV ^{40}K peak of Fig. 9.1); (3) ^{238}U=uranium via integrated count between 1.66 and 1.86 MeV (the so-called 1.76 MeV ^{214}Bi peak of Fig. 9.1); and ^{232}Th=thorium via integrated count between 2.42 and 2.81 MeV (the 2.62 MeV ^{208}Tl peak of Fig. 9.1).

9.6.3 Radon emanometers

Radon emanometry is concerned mainly with the detection and measurement of radon in soil and groundwater. Because radon is a noble gas, it does not form compounds with other elements and can move freely through pores, fissures, joints, and faults for distances up to several hundred meters. Radon will also dissolve in groundwater. Radon can have traveled a considerable distance from the source rocks of uranium before being detected.

In the **sniffer-type radon detectors** (grab-samplers), a hollow tube is inserted into the ground and a sample of the soil gas is pumped out into a container. This gas is then analyzed for its alpha activity by a zinc sulfide scintillometer device. Systems of this type, can also be used for sampling groundwater or surface water. Water samples are degassed and the gas–air mixture is analyzed to measure radon concentrations. Some environmental radon measurements require a continuous sampling of gas flux for studying temporal variations.

Integrating-type emanometers (e.g., the Track Etch) make use of alpha-sensitive cellulose nitrate film that is mounted to the inside bottom of a sampling cup. A number of such cups are buried below the ground surface, usually in a grid pattern over the survey area. The cups are left undisturbed over a period of several weeks, during which time alpha particles from radon in soil gas produce track-like damage on the film. The tracks are etched to make them visible and the density of the alpha tracks indicates the relative amount of radon at each sample station. Alpha Cup and Alpha Card are improved devices that are similar in principle to the Track Etch, but use a silicon semiconductor in place of the film. Due to higher collection efficiency and better counting geometry, these alpha devices have reduced burial periods (1–3 days) compared to etched-type devices which require integrating times of several weeks.

9.7 Field procedure and operational considerations

The Geiger counter is used only for foot traverses along a grid pattern of lines with the observer holding the detector some 40–50 cm above the ground. The scintillometer and the γ-ray spectrometer may be mounted in vehicles. These instruments record radiation intensities as counts per minute, but nowadays most of them are calibrated to determine the relative amounts of uranium or thorium by means of a standard source. Procedures of calibrating γ-ray spectrometers, for ground and airborne work, are discussed among others by Løvborg *et al.* (1977) and Grasty (1979).

The geometry of the outcropping formations has to be taken into account, because the instrument response is influenced by the source–detector separation as well as the source dimensions. Topographic irregularities, the dispersion of radioactive material due to weathering, and the background radiation are some of the factors affecting instrument readings. The 'background radiation' is due mainly to cosmic rays and the potassium content of local rocks, and it may vary from one area to another and also within a single area. Generally speaking, a reading is not considered significant unless it is three to four times the background.

Background radiation produced from the daughter products in the uranium decay series can be intense, and is time variant. As a disintegration product of ^{226}Ra (see Table 9.2), radon (^{222}Rn) may seep towards the surface with currents of water, diffuse through permeable rocks, or escape through fissures and cracks and thus be transported over considerable distances. ^{222}Rn, in turn, decays to ^{214}Bi which is the uranium indicator in γ-ray spectrometry (Fig. 9.1). Thus, migrated radon may give anomalous uranium indications which have no relation to uranium content of surface rocks or soil cover beneath the detector. However, detection of radon may be of importance by itself in detection of faults, fissures, and other features of environmental interest. Meteorological factors (temperature, barometric pressure, wind, and rainfall) also influence migration and accumulation of radon. An adequate assessment of these factors is important to interpretation of radon survey data.

More detailed accounts of field procedures and operational considerations in γ-ray spectrometry and radon emanometry can be found in Durrance (1986), Nielson *et al.* (1990), and Gregg and Holmes (1990).

9.8 Environmental concerns about radon

The primary concern surrounding environmental radioactivity is its effect on human health. The principal cause of concern has recently been ^{222}Rn (radon) that migrates from a geological environment to an indoor environment. The inhalation of Rn and its daughter products is thought to be the second leading cause of lung cancer following smoking. Radon in drinking water supplies may also be a cause of concern.

9.8.1 Generation of radon

Radon is a daughter product of radium, which in turn results from decay of uranium and thorium. Thus rocks and soils enriched in uranium and/or thorium (see Table 9.3) are likely sources for radon. The natural radon isotopes, ^{222}Rn, ^{220}Rn, and ^{219}Rn (all occurring as gas), stem from the ^{238}U, ^{232}Th, and ^{235}U decay series, respectively. The mobility of radon is a result of its gaseous state and inert chemical properties which allow it to move as a gas or dissolved in geofluids (e.g., water). The most abundant isotope, ^{222}Rn, has a half-life of 3.825 days and it can be detected and

measured with either alpha scintillometry or gamma spectrometry. The abundance of ^{222}Rn stems from the abundance of its parent element, ^{238}U, which is 138 times more abundant than ^{235}U. In the environmental context, the other two isotopes, ^{220}Rn and ^{219}Rn, are of little importance, because of their lesser abundances and shorter half-lives, compared with ^{222}Rn. Therefore, in the following discussion the term 'radon' (or the symbol Rn) refers always to ^{222}Rn.

9.8.2 Radon transport mechanisms

Radon can emanate from the ground at a rate which is dependent on the lithology of the bedrock, structural features such as faulting and jointing, soil physical and chemical properties, mode of transport (diffusion or fluid flow), and atmospheric influences such as precipitation, wind, and temperature. Radon is soluble in water and most significant movement in the subsurface is probably related to the transport of radon by groundwater flow (Andrews and Wood, 1972). From an environmental standpoint, it is important to elucidate the physical mechanisms that are responsible for radon transport from the subsurface to dwellings and buildings. These mechanisms have been discussed in detail by, among others, Nazaroff and Nero (1988) and Nazaroff (1992). Only a brief overview will be presented here.

Only a fraction of the Rn generated in the soil or in the rock matrix can reach the pore space and be transported away. The fraction of Rn leaving the generation point and entering the pore space is called the **emanation coefficient** and is dependent on the grain size and structure of the soil or of the rock, and on water saturation in the pore space. Very few data are available for the emanation coefficient. It is generally found to vary between 0.01 and 0.3 (i.e. 1–30% of the total radon generated), higher values usually occurring in weathered and altered rocks, and in loose soils. Water saturation can play a very important role by increasing the emanation coefficient.

Rn can be transported in two different ways: by **molecular diffusion** and by **advective air flow** in the underground region. The spatial difference of radon concentration that exists between the surface and underground induces a diffusive radon flow towards the surface. Also, an advective radon flow can be initiated if a spatial air-pressure difference exists in the underground region. The advective transport process is of greater importance than molecular diffusion because it gives Rn the chance to travel over large distances in the subsurface before its decay. Nazaroff (1992) discussed possible origins for an air-flow field in the underground region. He concludes that the advective flux is mostly due to the temperature difference between the underground region and the surface. For the special case of dwellings or buildings, the advective flow is induced by temperature differences between the free surface and the building due to wind or due to ventilation and heating inside the house.

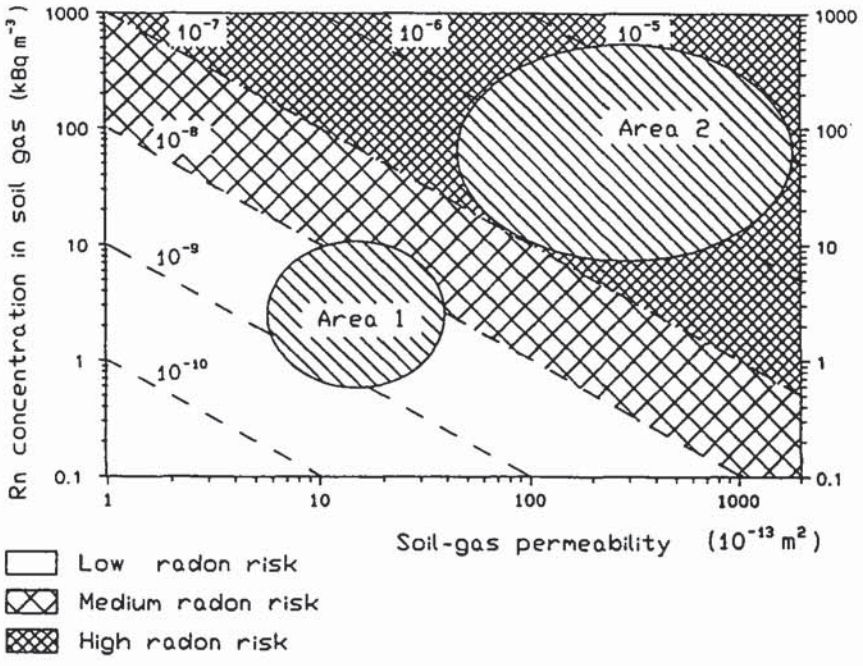

Fig. 9.2 Diagram showing the method to characterize various areas according to the different radon risk of soils. (After Medici and Rybach, 1994.)

9.8.3 Radon-risk index

Soil-gas permeability is one of the principal parameters, perhaps the dominant one, in controlling radon transport. The term 'soil' used here can be synonymous with vegetation cover, loose sediments, and hard rock. Several qualitative and semi-quantitative models of radon concentration in soil gas have been developed (LeGrand, 1987; Wilson, 1984), which use the geological and soil characteristics and measured radon concentration in soil gas to classify the area or site as high-risk, medium-risk, or low-risk from an environmental standpoint. To make an assessment of the radon risk of a specific soil in a given area, Medici and Rybach (1994) have introduced a **Rn-availability index** (RAV). This is defined by the product: Rn concentration in soil (Bq/m^3)×soil-gas permeability (m^2). Computed values of RAV can be used to characterize areas for their radon potential. Figure 9.2 shows the principle.

9.9 Examples of environmental radioactivity surveys

Environmental applications of radioactivity surveys include an assessment of the potential of indoor radon risk, soil and groundwater contamination, delineation of nuclear wastes and fallouts, mapping of faults, prediction of earthquakes, and monitoring of landslides.

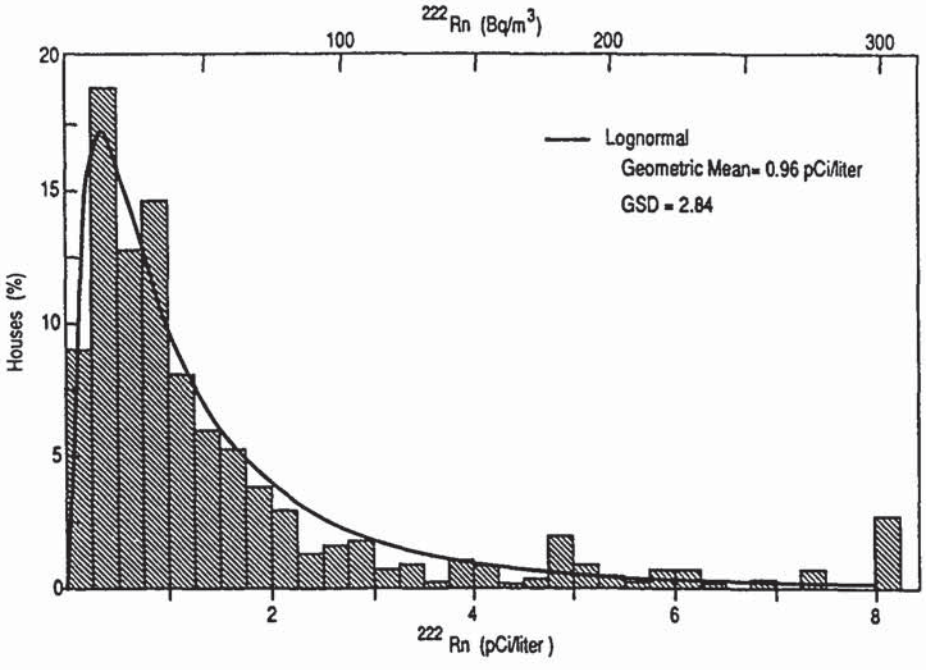

Fig. 9.3 Distribution of indoor radon concentrations in U.S. homes (After Nero *et al.*, 1986.)

9.9.1 Assessment of indoor radon risk and groundwater contamination

Radon in the domestic environment first drew wide attention when it was recognized that inhaling of Rn and Rn daughters can increase the risk of lung cancer.

Nero *et al.* (1986) compiled indoor radon concentration data from 552 single-family homes from 38 areas in the United States. The histogram distribution of their data shows a good agreement with the lognormal distribution curve (Fig. 9.3). This study suggested that about 7% of homes in the areas surveyed exceeded the EPA recommended limit of 4 pCi/l.

A radon study made at the Reading Prong site in Boyertown, Pennsylvania, U.S.A., showed that houses located over a uranium-rich quartz feldspar biotite gneiss generally have high radon concentrations of the order of 4 pCi/l to 200 pCi/l (Gundersen *et al.*, 1988). When this rock has been sheared, Rn in houses has generally been >200 pCi/l. This is a non-glaciated area, and soils have been derived through weathering of the underlying bedrock (gneiss). Samples of groundwater from this area also demonstrate that the highest concentrations of Rn (~100,000 pCi/l) are associated with the sheared gneiss. These concentrations are alarmingly high in view of the EPA potable water standard of 500 pCi/l (Section 9.3).

Another example of extremely high radon concentrations measured in soil and groundwater is from an area in the Piedmont Geologic Province of north Georgia, U.S.A., which is underlain by metamorphic rocks with thick soil (saprolite) cover.

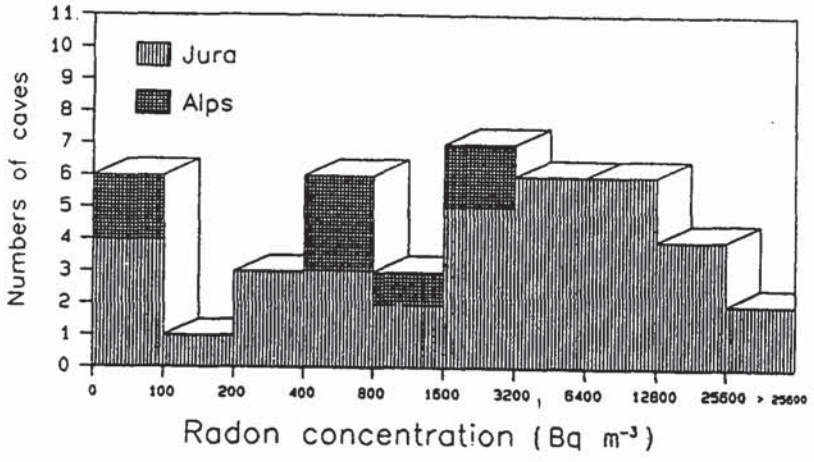

Fig. 9.4 Distribution of radon concentration in the air of selected Swiss karstic systems. Most of them are situated in the Jura mountains. Values up to 30,000 Bq/m³ were measured. Note the non-linear scale. (After Medici and Rybach, 1994.)

The highest measured values at some sites are reported to be 7900 pCi/l in soil gas and 840,000 pCi/l in groundwater (Gregg and Holmes, 1990). Radon concentrations of this magnitude present serious environmental problems.

Medici and Rybach (1994) reported a study that was made to assess the distribution of the indoor radon concentration in Swiss homes and to identify the local geological factors that influence the generation and transport of radon from the subsurface to buildings. The study was sponsored by the Swiss Federal Health Office under the program RAPROS (Radon Program Schweiz, 1987–1991). The data obtained from indoor radon measurements in living rooms of selected areas in different cantons of Switzerland showed average values <150 Bq/m³ in 90% of the homes and <500 Bq/m³ in 99% of them (N.B. 150 Bq/m³ is equivalent to 4pCi/l, the EPA recommended limit). In homes devoid of concrete base slabs in the cellars, the measured Rn concentration was found to be higher (often exceeding 1000 Bq/m³). The EC regulations recommend the limit of 400 Bq/m³ for existing buildings.

Another important observation reported in the Swiss study is that buildings positioned above karstified limestone rocks show anomalously high Rn concentrations, sometimes exceeding 10,000 Bq/m³. Figure 9.4 shows the distribution of Rn concentration in the air of 44 Swiss karst systems. In 34 cases the Rn concentration exceeds 400 Bq/m³. This Rn-charged air is able to travel over large distances through faults and cavities in the underground region. A model to explain the Rn transport in karstic areas was proposed by Surbeck and Medici (1990) and is shown schematically in Fig. 9.5. Percolating water in loose soil takes up Rn. When this Rn-charged water reaches a cave, Rn outgases from it, due to equilibrium factors. Rn is then free to migrate with the subsurface air and eventually to enter a building.

Finding the locations of buildings with high Rn concentrations is a major task

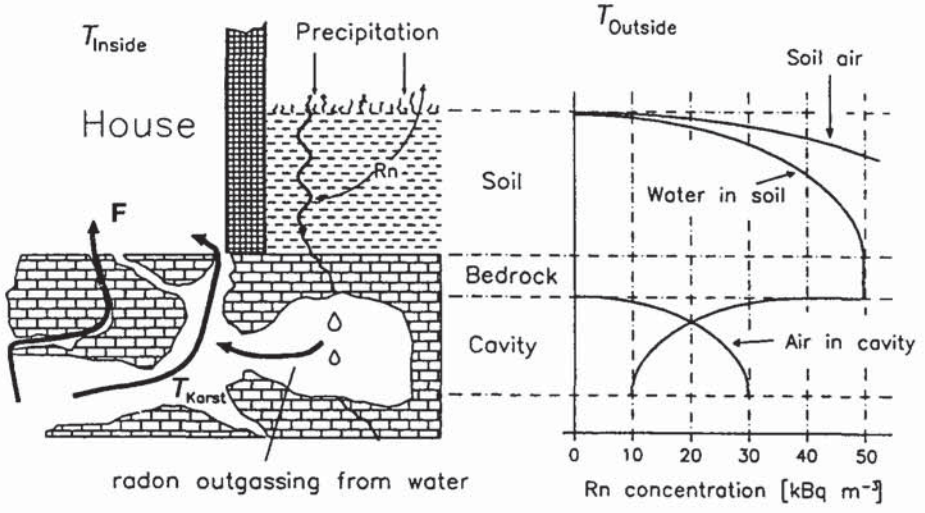

Fig. 9.5 Schematic model describing the radon cycle in karstic areas. The model can explain the elevated Rn concentration in many homes in the Jura region of Switzerland. (After Surbeck and Medici, 1990.)

for local environmental administrators. In such dwellings the Rn entry has to be mitigated by taking adequate measures. Procedures for prevention and mitigation of indoor radon are discussed in Mueller Associates *et al.* (1988).

9.9.2 Radiation from industrial and domestic waste dumps

An example of strong radiation coming from the industrial waste of uranium ore dressing is provided by the Vitro tailings site in Salt Lake City, Utah, U.S.A. This site had been in use for milling of uranium ore and vanadium ore from 1951 until 1968. The growing concern of health hazards due to radon emanation from the tailings site led the U.S. Department of Energy (Office of Operational Safety) to undertake an airborne radiometric survey of the Salt Lake valley in 1980. A system of 20 sodium iodide scintillators was deployed in a helicopter that flew the survey at 46 m altitude and 76 m line spacing. Since the processing of uranium ore leads to concentration of ^{226}Ra and other daughters, the total count data were also reduced to show equivalent radium concentrations. The coincidence of total count and radium anomalies was thought to have a high probability of delineating areas with uranium ore or tailings.

Figure 9.6 shows a portion of a map prepared from the survey data. The background radiation in the survey area varies between 9 and 16 μR/h. The tailings site shows the highest total count with exposure levels greater than 1400 μR/h. The western lobe of high radiation is thought to have resulted from wind-blown tailings. Other radiation anomalies along the railroad track were suggested as being caused by spilled material.

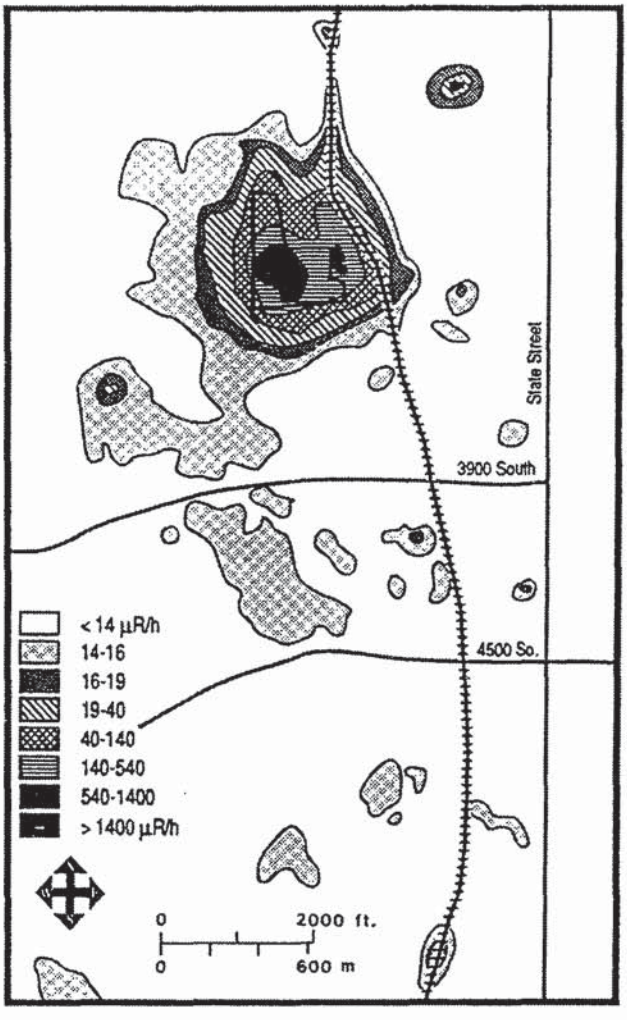

Fig. 9.6 Total exposure rate isopleths over the Vitro uranium milling site in Salt Lake City, Utah, U.S.A. The high-radiation zones in and around the tailings site (thick outline) are ten to several hundred times greater than the background radiation in this area which varies between 9 and 16 μR/h. (After Jobst, 1983.)

In eastern Europe, large areas of the former Soviet uranium mining industry are contaminated by radioactive material, warranting remedial actions. The latter can only mitigate the *impact* of radiation because radioactivity *cannot be destroyed* by chemical treatment or burning. Strong radiation can, though, be completely shielded by thick sealings of clay. Vogelsang (1995) gives an example of a 3-m thick clay sealing (Fig. 9.7) that absorbs γ-radiation of >75,000 Bq caused by a dump of uranium tailings. Over the uncovered slope, the radiation increases to a level of 75,000 Bq and a smaller increase occurs over the river bed where radioactive waste has accumulated.

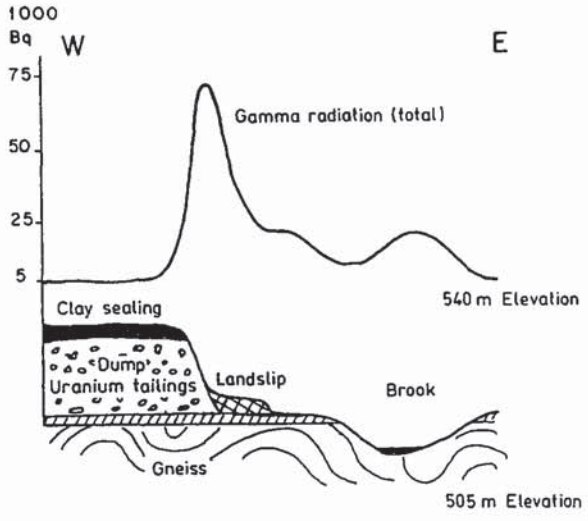

Fig. 9.7 Radiometric survey over a dump of uranium tailings partly covered by a 3-m thick clay sealing. (After Vogelsang, 1995.)

Domestic waste dumps usually show only weak radiation. The background effect caused by potassium-rich soil cover and surface rocks can be stronger than the radioactivity of domestic waste. Vogelsang made a study of the waste-disposal dump of the city of Hanover, Germany, by a radiometric helicopter survey and found no significant correlation between the radiation anomalies and heaps of domestic garbage.

9.9.3 Chernobyl radioactive fallout

This case study concerns detection and mapping of **radioactive fallout** over Sweden resulting from the accident at Chernobyl, Ukraine, April 26, 1986. The failure of the Soviet nuclear plant resulted in radioactive debris being carried by winds westward over Sweden where the mapping of debris was performed in detail. Vintersved *et al.* (1987) and Mellander (1988) have given vivid descriptions of the detection and monitoring work undertaken in Sweden to mitigate the effects of the radioactive fallout.

The first analysis of abnormal radioactivity was made from a sample analysis in Stockholm. The sample was a glass fiber filter through which 78,740 m^3 of ground level air had passed between 0710 April 25 and 0710 April 28, 1986. The measured concentration of non-natural radioactivity in air showed an enormous increase over the background level. During the night of April 28 and in the morning of April 29, a heavy rain fell over parts of Sweden. A car-borne detector found that the Gavle area received much more fallout than Stockholm where almost no rain fell.

To obtain an aerial distribution of the fallout, the Swedish Geological Survey commenced airborne radioactivity surveys at 150 m altitude. The results for the interval May 1–6, 1986 are shown in Fig. 9.8. The radiation anomaly shows a distinct

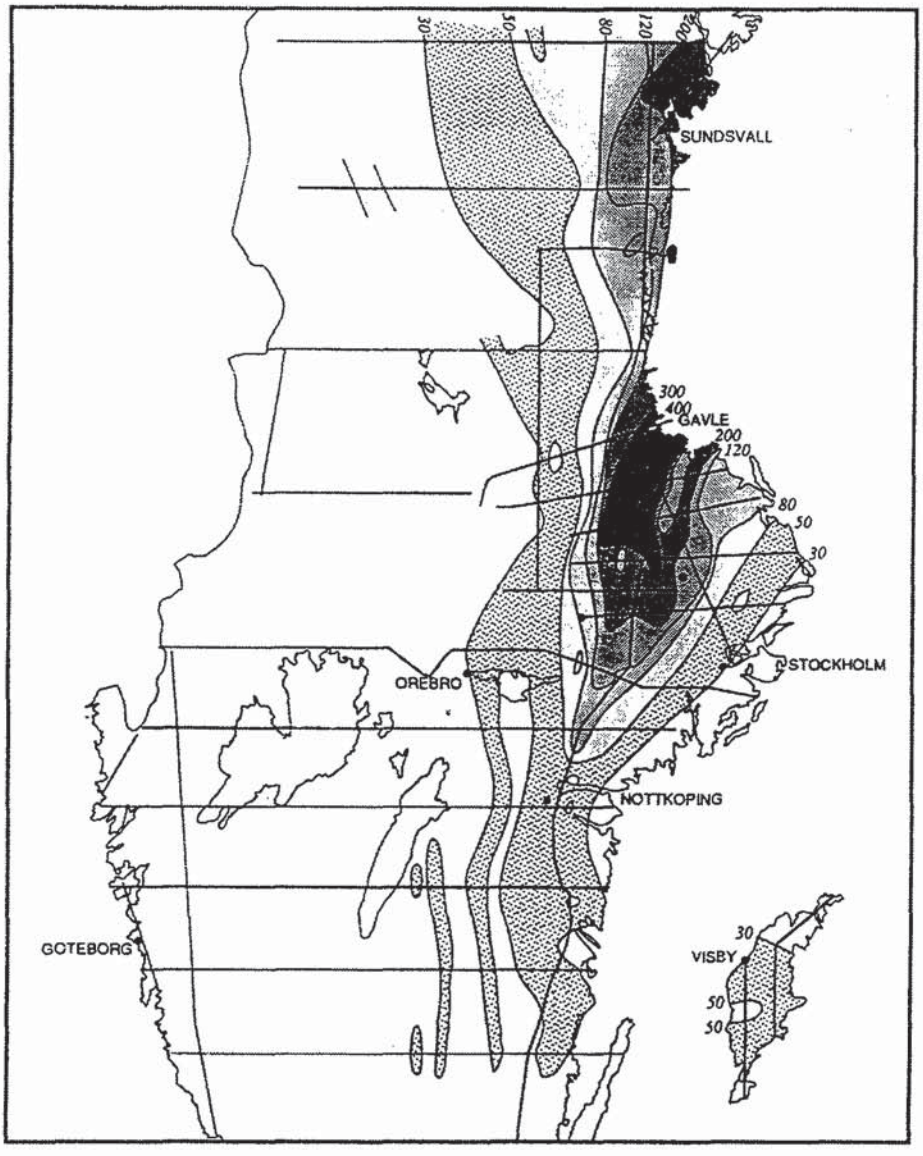

Fig. 9.8 Airborne γ-radiation map of northern part of Sweden for the interval May 1–6, 1986, after the Chernobyl fallout. The exposure rate values (μR/h) are indicated where the contours cross the coast line or edge of the map. (After Mellander, 1988.)

high exposure rate in the Gavle area, north of Stockholm. Between May 6 and May 8 the survey was extended to southern Sweden to discover whether or not dairy cows could be allowed to graze the fresh spring grass. In southern Sweden, where spring had progressed most, the situation was critical enough to warrant monitoring of environmental radioactivity.

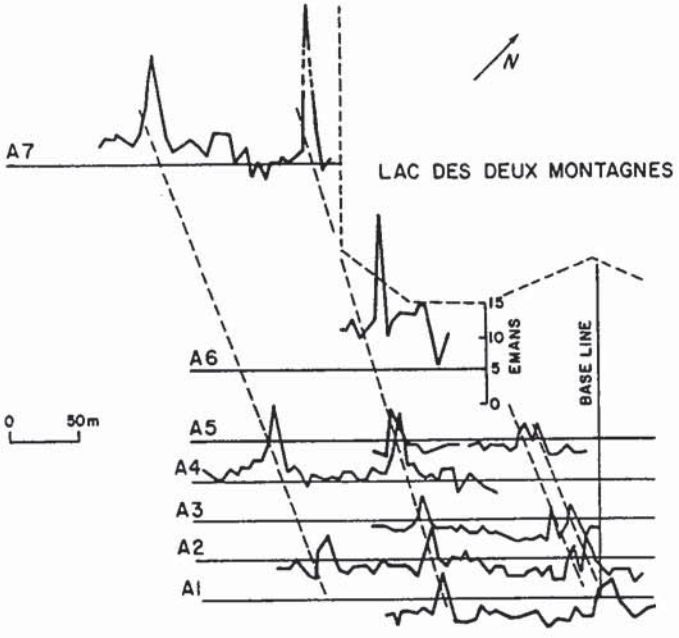

Fig. 9.9 Radon profiles at Point-aux-Carrieres, Montreal Island, Canada. Broken lines indicate inferred positions of fracture zones. 1 eman = 10^{-10} Ci/l. (After Abdoh and Pilkington, 1989.)

9.9.4 Detection of faults and fracture zones

Several studies have shown that faults and fracture zones are characterized by linear Rn anomalies caused by migration of radon through cracks and openings. Abdoh and Pilkington (1989) have given an example of a radon survey in the area of the Ile Bizard fault, Montreal Island, Canada. In this area the soil cover is thin and the bedrock is fully exposed along the northwest tip of Point-aux-Carrieres. The field measurements of the Rn content of soil gas were made using an ETR-1 pump-type emanometer. The sampling depth was kept constant at 0.6 m and the station spacing was 5 to 10 m on each profile. The results of the radon survey on traverses A1 to A7 are shown in Fig. 9.9. All profiles exhibit radon anomalies whose sources are believed to be associated with individual zones of fracture running parallel to each other. The observed linear trend of the Rn highs on the various profiles clearly indicates that the fractures associated with the Ile Bizard fault strike N60W in this area.

9.9.5 Radon-monitoring applied to earthquake prediction

The amount of radon in groundwater along active faults is commonly higher than what can be accounted for by radium dissolved in water, suggesting that radon generated in the rock matrix is constantly feeding into the aquifers. The possibility that radon concentrations in soil and groundwater may show earthquake-related

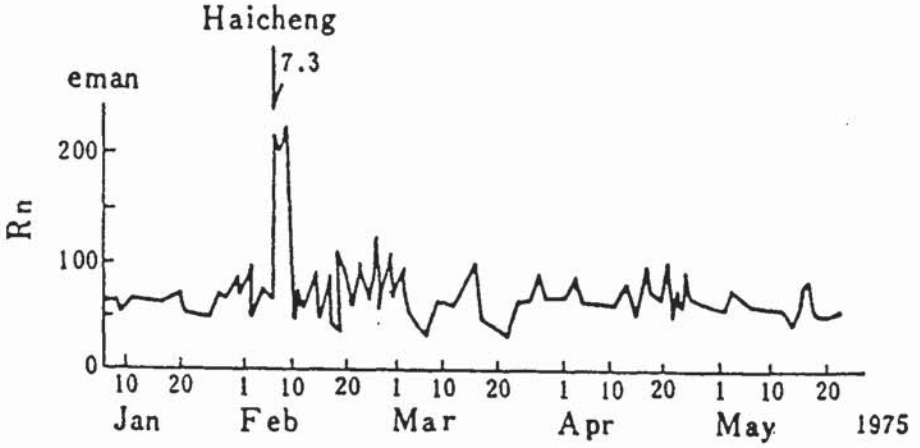

Fig. 9.10 Variation of radon content in water at the Tange hot spring in Liaoning province, China, before and after the Haicheng earthquake measured at an epicentral distance, $\Delta=72$ km. 1 eman$=10^{-10}$ Ci/l. (After Shi and Cai, 1986.)

changes has stimulated radon-monitoring efforts worldwide in earthquake prediction studies (King, 1986). This precursor phenomenon is thought to be related to initial episodes of strain release in the foreshock sequence that increase the emanation power of the rock due to fracturing.

Probably the most extensive monitoring of radon in groundwaters (at over 1000 sites) was made in China after the Xingtai earthquake (Richter magnitude, $M=7.2$) in 1966. Prior to the occurrence of earthquakes, anomalous radon changes (mostly increases) have been reported to be observed in monitoring wells at epicentral distances of up to several hundred kilometers. Among the most striking examples (Fig. 9.10) is the anomalous increase in the radon content in water at the Tanghe hot spring several hours before the occurrence of the Haicheng earthquake ($M=7.3$) on February 4, 1975 in northeast China. The radon anomaly, along with other precursory phenomena (increase in local seismicity, and unusual animal behavior) observed in the area, led to a successful prediction of the Haicheng earthquake. This precursory anomaly is significant in that the spring is located in an area of low radon concentration at the southern section of the Taizihe fault zone. Ordinarily, the permeability of the fault is low, and only a small quantity of radon-rich water may flow into the monitoring well. However it is possible that before the occurrence of the Haicheng earthquake, new cracks may have opened up along the fault which resulted in the flow of more radon-rich water into the monitoring well.

9.9.6 Investigations of landslide development

Landslides are associated with a great deal of surface fracturing and subsurface water flow. Studies made in the former U.S.S.R. have shown the possibility of using

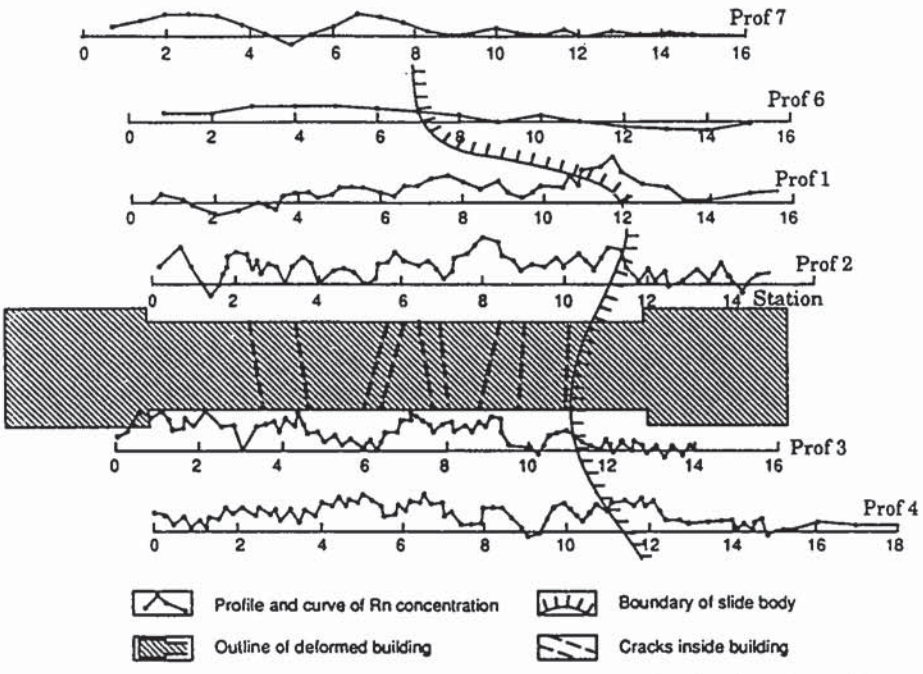

Fig. 9.11 Radon profiles in a landslide area, Lenin Hill, Moscow. (After Bondarenko *et al.*, 1983.)

radon methods to evaluate the stability of a slope, define the body of a landslide, and monitor the development of the landslide process.

Figure 9.11 shows a series of radon soil-gas profiles in a landslide area on Lenin Hill, Moscow. The building outlined in Fig. 9.11 had already suffered structural damage. The measured profiles show that within the sliding block, radon concentrations are generally higher than on the more stable soil to the right. There are other case histories showing similar relationships (Bondarenko *et al.*, 1983). These studies suggest that systematic radon measurements at different times can be used to monitor the development of a landslide from a stable state to an active state and back to a stable state.

9.9.7 Monitoring of radioactive contamination migration in subsurface

Use of radioactivity measuring probes in boreholes (Section 11.3.3) offers the possibility of monitoring migration of radioactive contaminants in flowing wells and aquifers. Nelson *et al.* (1983) reported a borehole logging study carried out at an experimental site for waste storage investigations in Stripa, Sweden. The initial objective of the study was to infer the rock mechanical and hydrophysical characteristics of the site. However, the anomalous behavior of the gamma logs (Fig. 9.12) prompted a closer study of the groundwater quality. The unexpected high gamma counts in the logs were recognized to be caused by the radon isotope ^{222}Rn. At the

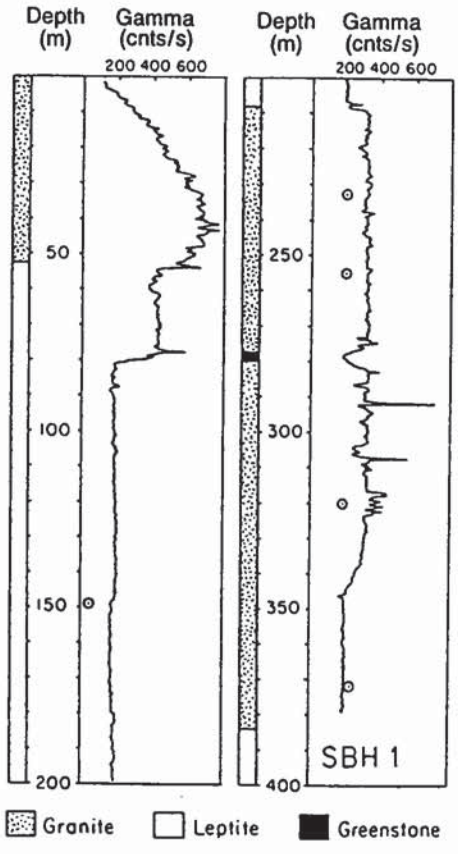

Fig. 9.12 Lithology and gamma logs of hole SBH-1, Stripa, Sweden, showing effects of radon gas. Circled data points represent background activities of the rocks calculated from laboratory spectral gamma analyses of core samples. (After Nelson *et al.*, 1983.)

Stripa site, it was determined that the radon in the groundwaters was derived from local granites containing relatively high concentrations (~40 ppm) of uranium. By analysis of repeated gamma logs conducted at regular intervals in the more seriously affected wells, it proved possible to trace the inflow, outflow, and movement of the waters charged with radon gas.

References

Abdoh, A. and Pilkington, M. 1989. Radon emanation studies of the Ile Bizard Fault, Montreal. *Geoexploration*, 25 341–54.

Andrews, J. H. and Wood, D. F. 1972. Mechanism of radon release in rock matrices and entry into groundwaters. *Trans. AIME B*, 81 198–209.

Bondarenko, V. M., Victorov, G. G., Demin, N. V., Kulkov, B. N., Lumpov, E. E. and Christich, V. A. 1983. *New Methods in Engineering Geophysics*. Nedra, Moscow.

Durrance, E. M. 1986. *Radioactivity in Geology – Principles and Application*. Holsted Press/John Wiley & Sons.

Grasty, R. L., 1979. Gamma-ray spectrometric methods in uranium exploration – theory and operational procedures. In Geol. Surv. Can., Econ. Geol. Rep., 31 147–61.

Grasty, R. L. 1987. *The Design, Construction, and Application of Airborne Gamma-ray Spectrometer Calibration Pads – Thailand*. Geol. Surv. Can., Paper 87-10.

Gregg, L. T. and Holmes, J. J. 1990. Radon detection and measurement in soil and groundwater. In *Geotechnical and Environmental Geophysics, Vol. 1*. Soc. Explor. Geophys., Tulsa, pp.251–62.

Gundersen, L. C. S., Reiner, G. M. and Agard, S. S. 1988. Correlation between geology, radon in soil gas, and indoor radon in the Reading Prong. In Marikos, M. A. and Hansman, R. H. (Eds.) *Geologic Causes of Natural Radioactive Nucleide Anomalies*. Missouri Dept. of Nat. Res., *Spec. Publ.*, 4:91–102.

Jobst, J. 1983. *Aerial Radiological Surveys of the Area Surrounding the Vitro Mill Site and Salt Lake City, Utah*. Las Vegas, NV, EG & G Survey Rep., NE-U-010.

King, C. Y. 1986. Gas geochemistry applied to earthquake prediction. *J. Geophys. Res.*, 91 12269–81.

LeGrand, H. E. 1987. A predictive model for indoor radon occurrence – a first approximation. In Graves, B. (Ed.) *Radon in Groundwater*. Nat. Water Well Assn., Lewis Publishers.

Løvborg, L., Grasty, R. L. and Kirkegaard, P. 1977. A guide to the calibration constants for aerial gamma-ray surveys in geoexploration. In *Amer. Nuclear Soc. Symp., Aerial Techniques for Environmental Monitoring, Las Vegas*.

Medici, F. and Rybach, L. 1994. Measurements of indoor radon concentrations and assessment of radiation exposure. *J. Appl. Geophys.*, 31 153–63.

Mellander, H. 1988. *Airborne Gamma Spectrometric Measurements of the Fallout over Sweden after the Nuclear Reactor Accident in Chernobyl, U.S.S.R.* Swedish Geological Company Rep. TFRAP 8803.

Mueller Associates, SPSCON Corp. 1988. *Handbook of Radon in Buildings*. Hemisphere Publishing Co.

Nazaroff, W. W. 1992. Radon transport from soil to air. *Rev. Geophys.*, 30(2) 137–60.

Nazaroff, W. W. and Nero A. V., Jr 1988. *Radon and its Decay Products in Indoor Air*. John Wiley & Sons, New York.

Nelson, P. H., Rachiele, R. and Smith, A. 1983. Transport of radon in flowing boreholes at Stripa, Sweden. *Trans. Amer. Geophys. Union*, 30 2395–405.

Nero, A. V., Schwehr, M. B., Nazaroff, W. W. and Revzan, K. L. 1986. Distribution of airborne radon-222 concentrations in U.S. homes. *Science*, 234 992–7.

Nielson, D. L., Linpei, C. and Ward, S. H. 1990. Gamma-ray spectrometry and radon emanometry in environmental geophysics. In *Geotechnical and Environmental Geophysics, Vol. 1*. Soc. Explor. Geophys., Tulsa, pp.219–50.

Shi, H. and Cai, Z. 1986. Geochemical characteristics of underground fluids in some active fault zones in China. *J. Geophys. Res.*, 91 12282–90.

Steiger, R. H. and Jaeger, E. 1977. Subcommision on Geochronology. Convention on the use of decay constants in geo- and cosmochronology. *Earth Planet. Sci. Lett.*, 36 359–62.

Surbeck, H. and Medici, F. 1990. Rn-222 transport from soil to karst caves by percolating water. In *Proc. 22nd Congr. IAH. Lausanne*, August 27–September 1.

Vintersved, I., DeGeer, L. E. and Bjurmann, B. 1987. Early measurements of the Chernobyl fallout in Sweden. *IEEE Trans. Nucl. Sci.*, NS-34 590–3.

Vogelsang, D. 1995. *Environmental Geophysics – A Practical Guide*. Springer-Verlag, Berlin, 173 pp.

Wilson, C. 1984. Mapping the radon risk of our environment: Indoor air. Vol. 2. Swedish Council for Building Res., pp.85–92.